

Numerical Analysis of Dolphin Kick in Competitive Swimming with Free Surface Effects

Ayato Takii¹, Naoki Kabuo², Masashi Yamakawa², Yusei Kobayashi²,
Shinichi Asao³, Seiichi Takeuchi³ and Makoto Tsubokura¹

¹ Kobe University, Kobe, Hyogo 657-0013, Japan

² Kyoto Institute of Technology, Sakyo-ku Kyoto 606-8585, Japan

³ College of Industrial Technology, Amagasaki Hyogo 661-0047, Japan
ayato.takii@penguin.kobe-u.ac.jp

Abstract. This study develops a high-precision numerical simulation method that considers free surface deformation to analyze fluid dynamics in dolphin kick swimming. We integrate an interface tracking method with the Moving Computational Domain (MCD) method and the unstructured moving-grid finite-volume method. The simulation validation demonstrates agreement with theoretical solutions, confirming the method's accuracy in analyzing flow fields with free surfaces. Using this approach, we analyze flow fields around dolphin kick swimmers and evaluate how gravity and free surface deformation affect propulsion and drag forces. The results indicate that the free surface experiences an upward displacement in front of the swimmer, a downward displacement above the back, and wave formation in the wake. Comparative analyses indicate that pressure distribution variations caused by gravity and vortex structures significantly influence propulsion and drag. Through simulations with varied joint angles and kick frequencies, we establish that swimming speed increases linearly with both joint angle amplification and stroke period reduction. Our analysis shows a proportional relationship between swimming velocity and the combined effect of increased joint angles and decreased kick cycle times. Our findings validate the effectiveness of the proposed simulation technique for determining optimal joint angles and stroke periods to achieve efficient swimming speeds in competitive dolphin kick swimming.

Keywords: Computational Fluid Dynamics, Free Surface, Moving Grid.

1 Introduction

Swimming is a premier event in the Olympic Games and garners worldwide attention. The pursuit of improved records is a critical objective for athletes and coaches alike, driven by advancements in swimming techniques and scientific methodologies. Since the late 20th century, scientific research has significantly contributed to improvements

in swimming performance. Counsilman [1] authored the first modern textbook on the science and techniques of swimming, catalyzing interest in this subject among numerous scientists. Over the past few decades, studies on propulsion, drag, kicking motions, and the effects of swimwear have been conducted using both experimental and numerical approaches. These scientific endeavors, coupled with the relentless efforts of athletes and coaches, have led to continuous updates of world records in swimming [2]. Further advancements in competitive records require the pursuit of optimal stroke techniques. In competitive swimming, rules pertaining to underwater swimming are pivotal. There is a common rule across freestyle, butterfly, and backstroke that requires swimmers to surface within 15 meters after the start and each turn [3]. This rule was instituted to prevent the proliferation of records due to excessive underwater swimming to maintain fairness and safety in the sport. Accurately understanding underwater propulsion within this limited 15-meter range is crucial for improving overall swimming records. Prior research has predominantly focused on the dolphin kick. For example, Lyttle et al. [4] measured drag during underwater motions after turns using towing experiments to estimate the optimal timing for initiating the kick. Additionally, Nakashima et al. [5] utilized simulations to investigate the impact of trunk undulations on swimming speed and propulsion efficiency during the dolphin kick. Experimental studies, such as that by Takagi et al. [6], have developed devices capable of measuring resistance without impeding the swimmer's motion, thereby quantifying both propulsion and drag. Concurrently, research using computational simulations has also advanced. Bixler et al. [7] demonstrated the utility of computational fluid dynamics (CFD) by modeling the hand. Furthermore, Nakashima et al. [8] developed a comprehensive human body simulation model (SWUM) aimed at resolving hydrodynamic issues in swimming. Webb et al. [9] also examined the effects of swimsuits on race times through simulations. However, experimental techniques are limited in capturing the detailed flow around a swimmer due to the influence of measuring devices and constraints on measurable areas. In contrast, simulation methods can potentially overcome these limitations and analyze detailed flow fields and their effects on the human body. While current CFD analyses show good agreement with experimental data, examples rigorously handling free surfaces are scarce. As the dolphin kick involves surfacing from approximately one meter below, the effect of free surface deformation on the swimmer is significant. Research addressing free surfaces includes studies by Cohen et al. [10] using the SPH method and Chen et al. [11] using the VOF method. To tackle these challenges, this study adopts an interface tracking method, which directly represents the free surface by deforming the computational grid. Compared to interface capturing methods, interface tracking offers higher computational accuracy by directly representing the interface [12]. Furthermore, by integrating this method with the Moving Computational Domain (MCD) method [14], which we have been developing in our laboratory, and the unstructured moving-grid finite-volume method that satisfies conservation laws in computations involving movement and deformation [13], we aim to establish a simulation environment capable of handling swimmer acceleration, deceleration, and complex movements. The objective of this research is to contribute to the enhancement of dolphin kick performance in competitive swimming. Specifically, to conduct highly accurate and realistic simulations that account for water surface deformation, we develop a

simulation technique that applies the interface tracking method to the MCD method and the moving-grid finite-volume method and validate its effectiveness. Subsequently, we simulate dolphin kick swimmers and compare and analyze the effects of various parameters, such as water surface deformation, gravity, and dolphin kick form, on fluid behavior to demonstrate the utility of our developed technique. The simulation method proposed in this study is expected to elucidate the detailed fluid behavior of the dolphin kick in competitive swimming and contribute to improving athlete performance. In particular, analyses that consider free surface deformation enable simulations under more realistic conditions and are expected to yield new insights.

2 Numerical Approach

2.1 Governing Equation

The governing equations for water flow consist of the continuity equation and the three-dimensional incompressible Navier-Stokes equations:

$$\frac{\partial u}{\partial x} + \frac{\partial v}{\partial y} + \frac{\partial w}{\partial z} = 0, \quad (1)$$

$$\frac{\partial \mathbf{q}}{\partial t} + \frac{\partial \mathbf{E}}{\partial x} + \frac{\partial \mathbf{F}}{\partial y} + \frac{\partial \mathbf{G}}{\partial z} = \left(\frac{\partial \mathbf{E}_V}{\partial x} + \frac{\partial \mathbf{F}_V}{\partial y} + \frac{\partial \mathbf{G}_V}{\partial z} \right) + \mathbf{H}_g, \quad (2)$$

where

$$\mathbf{q} = \begin{bmatrix} u \\ v \\ w \end{bmatrix}, \mathbf{E} = \begin{bmatrix} u^2 + p \\ uv \\ uw \end{bmatrix}, \mathbf{F} = \begin{bmatrix} uv \\ v^2 + p \\ vw \end{bmatrix}, \mathbf{G} = \begin{bmatrix} uw \\ vw \\ w^2 + p \end{bmatrix} \\ \mathbf{E}_V = \frac{1}{Re} \begin{bmatrix} u_x \\ v_x \\ w_x \end{bmatrix}, \mathbf{F}_V = \frac{1}{Re} \begin{bmatrix} u_y \\ v_y \\ w_y \end{bmatrix}, \mathbf{G}_V = \frac{1}{Re} \begin{bmatrix} u_z \\ v_z \\ w_z \end{bmatrix}, \mathbf{H}_g = \begin{bmatrix} 0 \\ -1/Fr^2 \\ 0 \end{bmatrix} \quad (3)$$

u, v, w are the corresponding velocity components in the x, y, z direction, respectively, t is time, p is pressure and Re is the Reynolds number with the representative length that is half width of mouth ($= 0.02$ m) and the representative velocity ($= 12.0$ m/s). Additionally, $\mathbf{E}, \mathbf{F}, \mathbf{G}$ are the advection vectors, $\mathbf{E}_V, \mathbf{F}_V, \mathbf{G}_V$ are the corresponding viscous stress vectors, and \mathbf{H}_g is the external force with the Froude number Fr . Physical variables are defined at cell centers. The governing equations are solved using an in-house code based on the Moving-Grid Finite-Volume Method with an unstructured grid. This method guarantees the satisfaction of geometrical conservation laws even when the computational grid undergoes deformation. The specific details are provided in the literature [15]. To solve the incompressible flow, the fractional step method is employed, combined with implicit temporal discretization using the Crank-Nicolson scheme for both inviscid and viscous fluxes. In the first step, the linear systems for tentative velocity are solved using the LU-SGS (Lower-Upper Symmetric-Gauss-Seidel) method [16]. In the second step, the Poisson equation for pressure is solved using the SOR (Successive Over Relaxation) method.

2.2 Motion Equation for Swimmer

We perform a coupled simulation wherein a swimmer propels themselves through fluid interaction. Specifically, we compute the swimmer's displacement at each time step using the known hydrodynamic forces acting on the swimmer's body surface from the previous time step. While a swimmer naturally exhibits six degrees of freedom in translational and rotational motion, this simulation simplifies the analysis by solving a one degree of freedom equation of motion along the forward direction only. This simplification is implemented to facilitate the observation of the impact of human body motion on free surface deformation and propulsion forces.

$$m \frac{dx^2}{dt^2} = F_x. \quad (4)$$

To accurately represent the swimmer's movement, the Moving Computational Domain (MCD) method is adopted, wherein the computational domain translates with the moving object. This approach eliminates the need to regenerate the entire computational grid for each movement, requiring only the creation of grid in the vicinity of the object. Furthermore, although the computational grid itself is moving, the governing equations remain formulated within an inertial frame of reference. This eliminates the need to evaluate centrifugal and Coriolis forces, thereby simplifying the implementation of the equations of motion.

2.3 Interface tracking method

The flow induced by human body motion propagates to the water surface, causing interface deformation. In this study, we utilize an interface tracking method, where the interface is represented by grid deformation. Specifically, we assume that the interface can be described by a height function. Here, the superscript n denotes the time step. For grid points on the interface, the following relationship holds at each time step:

$$h(x^n, y^n, t^n) = z^n, h(x^{n+1}, y^{n+1}, t^{n+1}) = z^{n+1}. \quad (5)$$

Performing a Taylor series expansion of this equation and neglecting terms of second order and higher, we obtain the following:

$$\frac{\partial h}{\partial t} + u \frac{\partial h}{\partial x} + v \frac{\partial h}{\partial y} = w, \quad (6)$$

The water surface is then represented by deforming the surface grid based on the interface height obtained by solving this equation. Note that surface tension is neglected in this computation. Furthermore, it is necessary to smoothly deform the surrounding computational grid in response to this interface deformation. In this study, we employ a spring analogy method [17] to maintain an appropriate shape for the computational grid.

3 Validation of Interface Tracking Method

In this chapter, we validate the interface tracking method by comparing the free surface deformation of a rotating cylindrical fluid with an analytical solution. As the computational domain, we created a cylindrical container as shown in Fig. 1(a). The cylinder has a diameter of 1, and the number of elements is approximately 700,000. The analytical solution for the displacement Δh of the free surface from its initial position, with r representing the distance from the rotation axis, is given by the following equation:

$$\Delta h = \frac{(2r^2 - R^2)\omega^2}{4g}, \quad (7)$$

where R is the cylinder radius and ω is the rotational angular velocity. The computational conditions were set as follows: an angular velocity ω of $\pi/2$, a Reynolds number of 100, and a Froude number of 1.0. Fig. 1(b) illustrates the free surface height of both the exact solution and the computed result converged to a steady state. It can be observed that the height of the reference points on the free surface closely matches the analytical solution. The largest deviation occurred at the point $r = \pm 0.125$, with a relative error of approximately 2.6% with respect to the maximum height difference of the water surface.

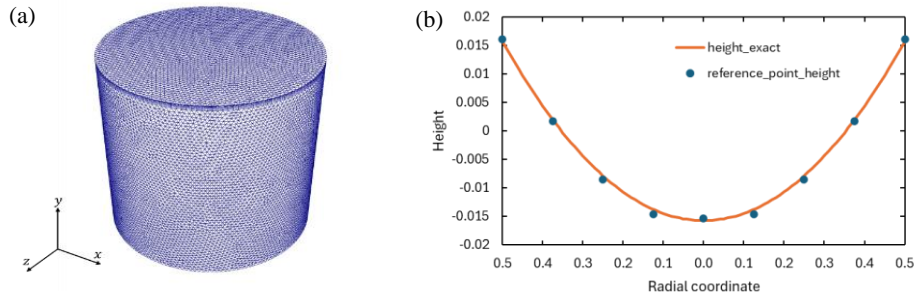


Fig. 1. (a) Computational grid of a rotating cylindrical container. (b) Comparison between the computed free surface height and the analytical solution

4 Fluid Analysis of a Dolphin Kick Swimmer

4.1 Numerical Setup

In this chapter, we conduct a flow analysis around a swimmer performing the dolphin kick technique. The human body model and swimming motion data used in this study are based on footage of a male competitive swimmer performing the dolphin kick, as depicted in Fig. 2(a), consistent with prior research [18]. The swimmer in question

has an extended glide posture length of 2.2 m and a body weight of 65 kg. As illustrated in the figure, seven joint points are defined: fingertips, shoulders, back, waist, knees, ankles, and toes. Subsequently, the coordinates of each joint point were measured from 27 frames of images spanning one cycle of the dolphin kick motion, and the joint angles 1 through 5 in Fig. 2(a) were calculated. Spline interpolation was then applied to these calculated joint angles to determine the joint angles at any given time. However, due to the difficulty in avoiding distortion of the water surface grid caused by grid deformation around the swimmer positioned underwater, the measured angles were restricted to approximately one-third in this study. The temporal changes in each joint angle used in this study are shown in Fig. 2(b), where the horizontal axis represents time within one cycle and the vertical axis represents the joint angle. It is evident that the knee flexion exhibits the most significant angular change, with maximum flexion at $t/T = 0.67$ and full extension at $t/T = 0.89$. The period of one cycle of the dolphin kick is 0.65 seconds. Fig. 3 illustrates the swimmer model with varied joint angles. Fig. 4 shows the computational domain used for the numerical simulation. Fig. 5 presents a cross-sectional view of the three-dimensional computational grid in the vicinity of the swimmer. The number of elements is 3,816,267 cells. Next, the swimming conditions are described. From the start of the calculation until $t = 0.8$ seconds, the swimmer accelerates to a forward speed of v while in an extended glide posture. Subsequently, the swimmer slows down due to drag while maintaining the same posture until $t = 1.0$ seconds. This replicates the initial velocity obtained from pushing off the wall in competitive swimming. After $t = 1.0$ seconds, the dolphin kick motion is initiated. The representative values used in the calculation are as follows: the full length of the swimmer in an extended glide posture (2.2 m), the swimmer's velocity during the dolphin kick motion obtained from the video data (1.85 m/s), the density of water at 28 degrees Celsius (996.2 kg/m^3), and the viscosity coefficient ($8.329 \times 10^{-4} \text{ Pa} \cdot \text{s}$).

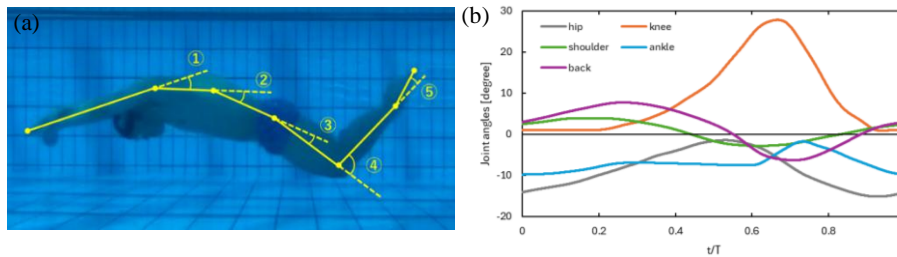


Fig. 2. (a) Dolphin kick motion performed by a competitive swimmer and (b) temporal variations in joint angles during one kick cycle

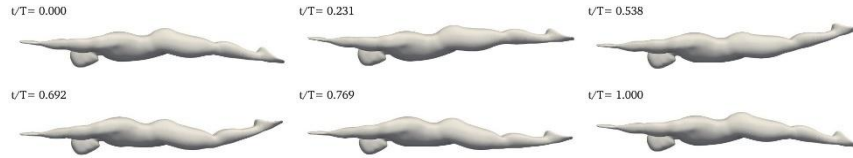


Fig. 3. Postures of the swimmer during the dolphin kick motion

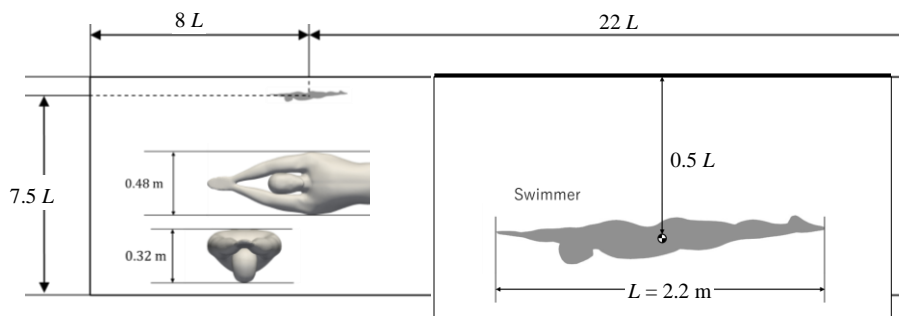


Fig. 4. Computational model of the swimmer in a streamlined glide position

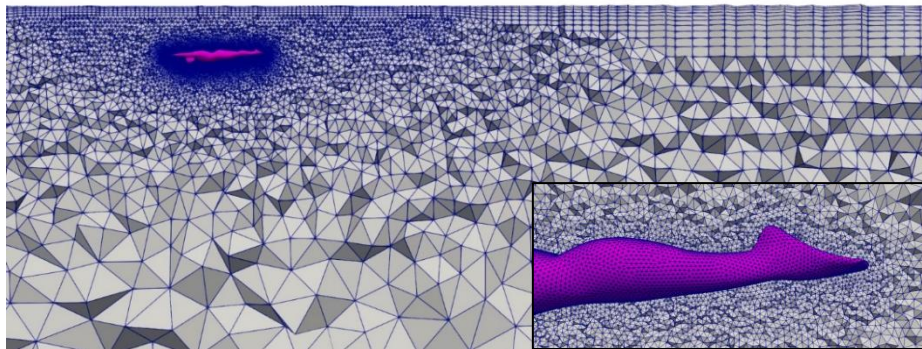


Fig. 5. Cross-sectional view of the three-dimensional computational grid near the swimmer, along with a close-up view of the grid around the legs

4.2 Effects of Gravity and Free Surface

In this section, we compare numerical analyses of two cases: one without gravity and free surface deformation (Case 1) and another with both gravity and free surface deformation applied (Case 2: $Fr = 0.3983$). The boundary conditions for Case 1 were set as

follows: no-slip condition for the swimmer, slip condition in the spanwise direction, inflow at the front, and outflow at the rear and bottom surfaces. For Case 2, the boundary conditions were identical to Case 1, except that the pressure at the bottom and rear surfaces was determined based on the water depth at the cell face center coordinates. Fig. 6 illustrates the pressure distribution and free surface shape at the $z = 0$ cross-section at $t = 1.5$ s (during the down-kick motion). The pressure values represent dynamic pressure, with hydrostatic pressure subtracted. The pressure distribution reveals a significant negative pressure region behind the swimmer's feet. This suggests the generation of vortices in the wake of the legs, which substantially contributes to the swimmer's propulsion.

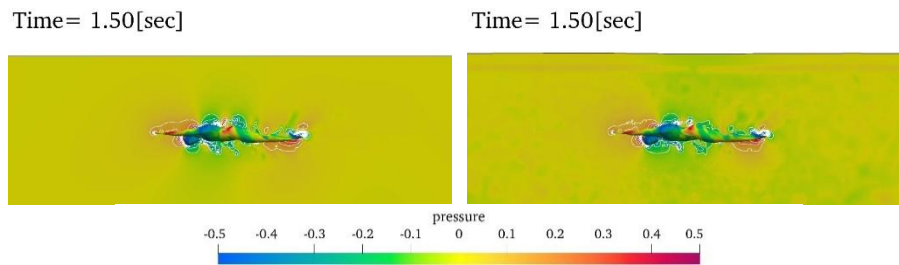


Fig. 6. Comparison of pressure distributions and free surface deformations:(left) Case 1 without gravity and free surface effects, (right) Case 2 with gravity and free surface effects

The free surface shape, although exhibiting minor displacements, shows an elevation in front of the swimmer, a depression near the upper back, and the formation of wave patterns towards the wake. This is likely attributed to the high-pressure zone around the swimmer's head and shoulders, and the low-pressure zone due to the curvature of the back, which is reasonable for free surface deformation induced by the motion of a submerged object. Fig. 7 details the velocity changes over two dolphin kick cycles: (a) the second and third cycles ($t = 1.65$ – 2.95 s) with significant velocity variations, and (b) the tenth and eleventh cycles ($t = 6.85$ – 8.15 s) where the velocity approaches a steady state. The horizontal axis of each graph represents the time within the cycle, with the start of the dolphin kick defined as 0. The left vertical axis represents the swimmer's velocity, and the right vertical axis shows the velocity difference between Case 1 and Case 2. Gray dashed lines indicate the boundaries of the dolphin kick cycles. We now discuss the velocity difference between the two cases. In the deceleration phase shown in Fig. 7(a), the water resistance dominates over the propulsion force, necessitating consideration of the high-pressure influence from the swimmer's front. In Case 2, at the start of the dolphin kick ($t = 1$ s), the free surface above the swimmer's head exhibits a displacement of approximately $+0.2\%$ relative to the swimmer's depth, while the free surface directly above the legs shows a displacement of approximately -0.9% . This free surface deformation likely induces a pressure difference due to gravity in the swimmer's front-rear (x-axis) direction compared to Case 1, thereby amplifying the velocity

difference. Additionally, the flow from the high-pressure to low-pressure regions acts in a direction that impedes the swimmer's progress.

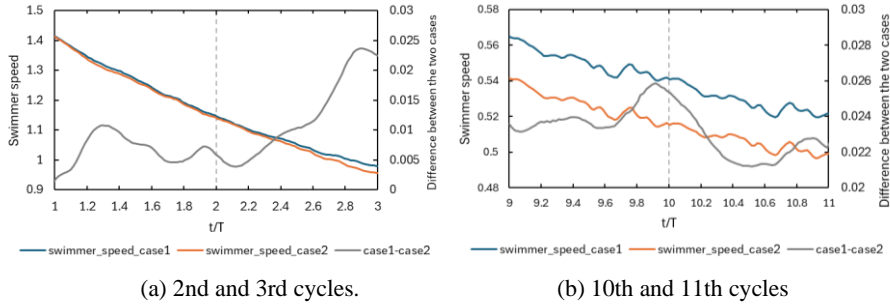


Fig. 7. Temporal variations in swimmer velocity for Case 1 and Case 2

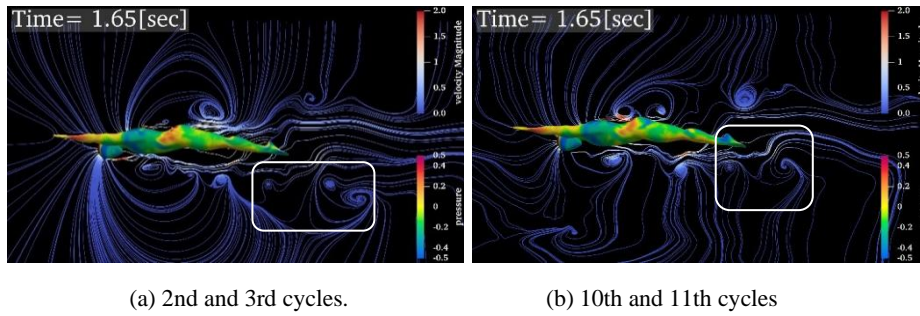


Fig. 8. Streamlines around the swimmer at the end of one dolphin kick cycle

Fig. 8 displays the streamlines around the swimmer after one dolphin kick cycle ($t = 1.65$ s, $t/T = 1.0$). In both cases, flow separation occurs near the swimmer's shoulders and head, leading to vortex formation. In the dolphin kick motion, the effective capture of these vortices by the legs is crucial for propulsion, not merely the displacement of water. The white box in the figure highlights the vortices captured during the first cycle of the dolphin kick. In Case 1, the vortices are ejected into the wake, whereas in Case 2, they tend to remain in place. This difference in vortex behavior is likely a contributing factor to the velocity difference observed in the second cycle in Fig. 7(a). These results suggest that gravity and free surface deformation modify the hydrostatic pressure gradient, influencing the swimmer's propulsion and drag forces. Furthermore, we confirmed that differences arise in the distribution of vortices, which significantly contribute to propulsion, and their impact on the swimmer.

4.3 Effects of Joint Angle Variation

In this section, we conduct simulations with increased joint range of motion and analyze the resistance and propulsion forces. It is important to note that all cases presented

below include numerical computations that account for gravity and free surface deformation. The joint angles are increased to 1.5 times and 2.0 times those of Case 2, denoted as Case 3 and Case 4, respectively. Fig. 9 illustrates the pressure distribution and free surface shape around the swimmer for Case 3 and Case 4. The white lines in the figures represent pressure contour lines. The pressure values represent the dynamic pressure, with the hydrostatic pressure subtracted. From the figures, it is observed that Case 3 and Case 4 exhibit similar trends in pressure distribution and free surface deformation around the swimmer as Case 2. However, significant differences appear in the pressure near the legs due to the dolphin kick motion, particularly at $t = 2.0$ s, during the initial phase of the down-kick motion. Furthermore, at $t = 3.0$ s, pressure due to the toroidal vortices generated after the down-kick motion can be observed, and differences in the size of these vortices are also confirmed. However, no significant differences in free surface deformation were observed compared to Case 2.

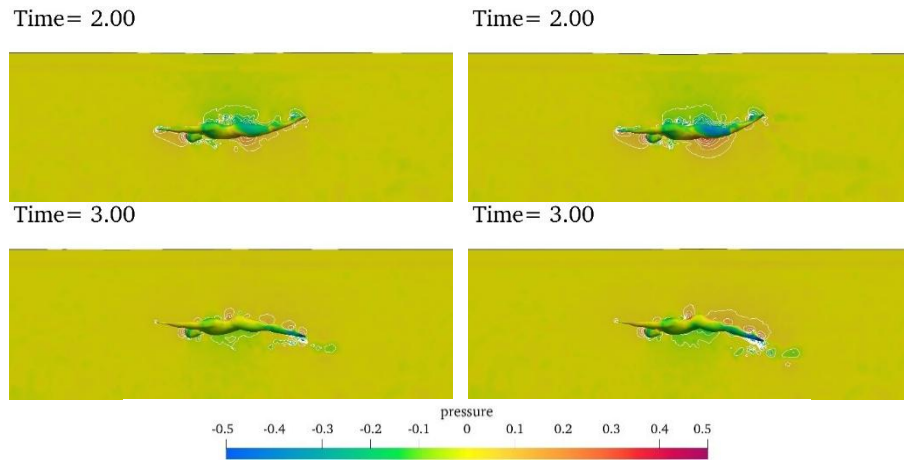


Fig. 9. Comparison of pressure distributions and free surface deformations for: (left) Case 3 (joint angles increased by 1.5 \times), (right) Case 4 (joint angles increased by 2.0 \times)

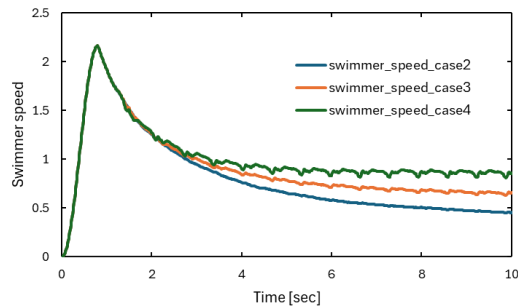


Fig. 10. Comparison of swimmer velocity for Cases 2, 3, and 4

Fig. 10 illustrates the temporal variation of the swimmer's dimensionless velocity for each case. As the joint angles increase, the final velocity rises. The average velocity during one cycle after reaching equilibrium is 1.495 times higher for Case 3 compared to Case 2, and 1.982 times higher for Case 4 compared to Case 2, indicating a near-linear relationship with the joint angle magnification. This suggests a proportional relationship exists between the two up to a certain degree of angle change, with the increase in propulsion force exceeding the increase in drag. We now focus on the first cycle of the dolphin kick.

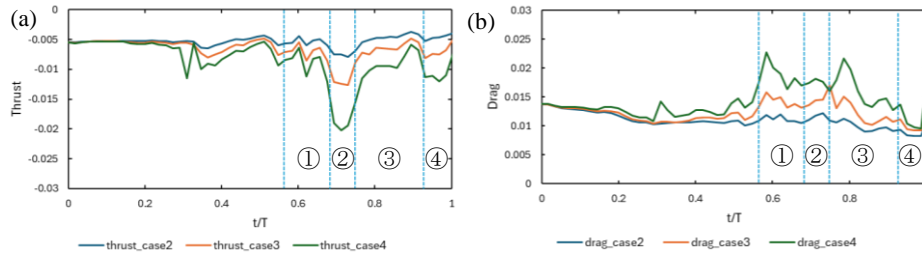


Fig. 11. Time histories of (a) propulsion force, (b) drag force during the first kick cycle

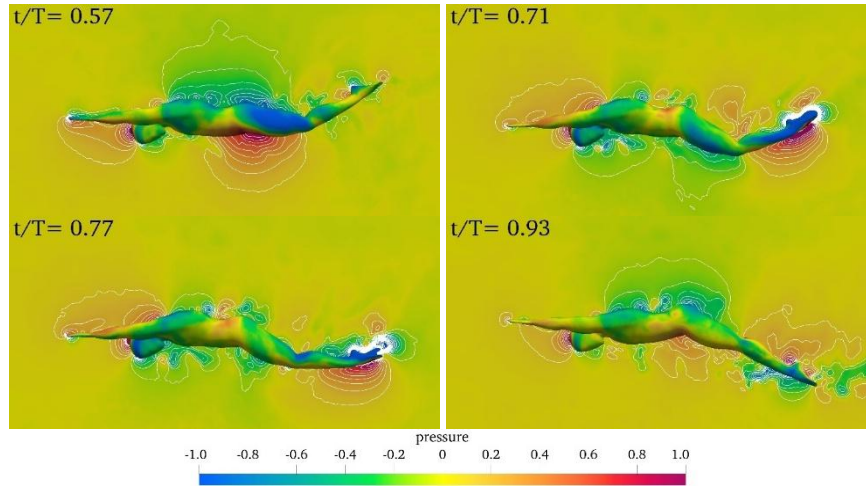


Fig. 12. Pressure distributions around the swimmer at different time steps (t_1, t_2, t_3, t_4) during the first kick cycle in Case 4

Fig. 11 shows the swimmer's propulsion and drag forces during this cycle. Here, since the swimmer's direction of motion is in the negative x-axis direction, the force in the negative direction is defined as propulsion force, and the force in the positive direction

is defined as drag force. Each horizontal axis, t/T , represents the time in the dolphin kick cycle, with the start of the dolphin kick defined as 0. In real-time, this corresponds to 1 second to 1.65 seconds. The four points indicated by light blue dashed lines ($t_1 = 0.57, t_2 = 0.71, t_3 = 0.77, t_4 = 0.93$) represent the intervals during the down-kick motion where a velocity difference occurs between Case 2 and Case 4. These intervals are labeled ① through ④. Fig. 12 shows the pressure distribution at times t_1 through t_4 . From Fig. 12, the following observations can be made. Interval ①: Due to deformation of the hip joint, the thigh tilts forward, creating resistance against the flow from the front. The undulation of the swimmer's core also contributes to propulsion, increasing not only resistance but also propulsion. However, in the first cycle of the dolphin kick, immediately after acceleration, the swimmer's speed is high, making resistance predominant. Interval ②: Extension of the lower leg pushes water rearward, gaining propulsion from its reaction force. Similar to Interval ①, the swimmer's frontal area remains larger compared to Case 2, leading to increased resistance, yet Fig. 11 shows approximately twice the propulsion force. However, as knee extension progresses, efficient force reception in the direction of travel diminishes, passing the peak propulsion force. Interval ③: As knee extension concludes, the peak resistance occurs the moment propulsion force from reaction ceases. Nevertheless, Fig. 11 reveals force from the rear of the leg due to the vortex formed during the downward kick. Interval ④: Entering the upward kick generates propulsion force. In summary, Case 4 demonstrates deceleration in Interval ①, acceleration in Interval ②, minor deceleration in Interval ③, and acceleration in Interval ④ compared to Case 2. Similar behavior was observed during the steady speed phase with minimal velocity changes in the 9th cycle (6.2-6.85 seconds). A notable difference was the increased propulsion force due to the downward kick. Resistance exhibits two peaks during thigh tilting and after knee extension, though their values are smaller. However, additional peaks were confirmed with increased joint angles. Therefore, selecting joint angles corresponding to surrounding flow velocities is crucial for efficiently capturing water during the dolphin kick. From these results, to achieve propulsion throughout the swimming motion, it is necessary to vary joint angles during stages where speed increases rapidly after the start or turn and during stages where speed stabilizes, to obtain optimal propulsion and resistance in each speed regime.

4.4 Influence of Dolphin Kick Frequency

In this section, we examine cases where the dolphin kick cycle time (T) is reduced to 80% and 60% of its original value. Since the dolphin kick cycle time in Case 2 is $T = 0.65$ seconds, the reduced cycle times are $T = 0.52$ seconds and $T = 0.39$ seconds, respectively. Similarly, for Cases 3 and 4, where the swimming motion is increased by 1.5 and 2 times, respectively, calculations are performed with these reduced cycle times. Specifically, for joint angles in Cases 2-4, conditions with an 80% cycle time are

denoted as Cases 5-7, and conditions with a 60% cycle time as Cases 8-10. The computational results, particularly the temporal variation of the swimmer's dimensionless velocity for the 1x and 2x motion increase cases, are shown in Fig. 13. It is observed that reducing the repetition cycle time leads to an increase in velocity.

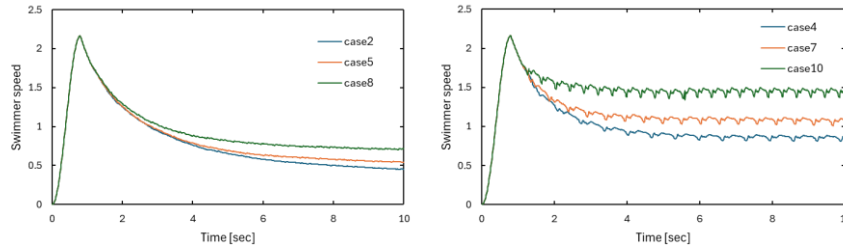


Fig. 13. Comparison of swimmer velocity for different kick frequencies: Cases 2, 5, and 8 (angle ratio $\times 1$), Cases 4, 7, and 10 (angle ratio $\times 2$)

Next, we define α/β , where α is the joint angle amplification factor and β is the dolphin kick cycle frequency factor. Furthermore, we consider the average velocity in each case, normalized by the average velocity of Case 2. These relationships are illustrated in Fig. 14. Note that the average velocity is calculated using the velocity after reaching equilibrium. From Fig. 14, it is evident that the swimmer's average velocity is approximately proportional to α/β . From these results, it is clear that changing the joint angles and the dolphin kick cycle time results in a nearly linear increase in the swimmer's final velocity, depending on each factor. However, it is predicted that as the dolphin kick motion becomes significantly faster, the effect of deceleration due to the average drag force will outweigh the acceleration due to the maximum propulsion force, leading to a reduction in efficient swimming speed.

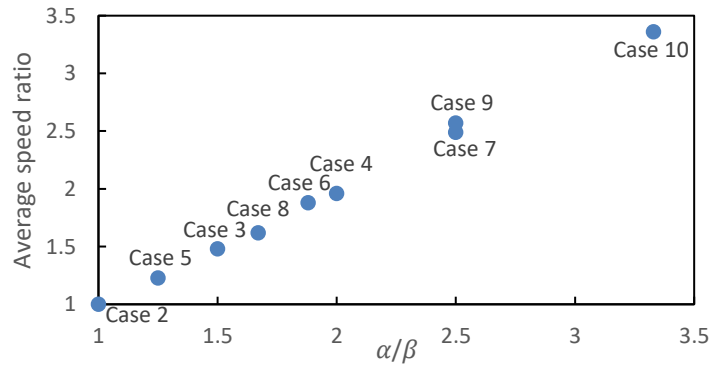


Fig. 14. Relationship between normalized average swimming speed and the ratio of joint angle amplification factor α to kick cycle frequency factor β

5 Conclusions

In this study, with the objective of enhancing the accuracy of swimming simulations, we proposed an analytical method using the moving-grid finite-volume method that accounts for gravity and free surface deformation. Employing the proposed method, we simulated the flow field around a dolphin kick swimmer undergoing dynamic acceleration and deceleration underwater, demonstrating its utility through a comparison with conventional methods that disregard gravity and free surfaces. Furthermore, based on simulations that varied the motion parameters of the dolphin kick, we conducted a comparative analysis, resulting in the following conclusions. The proposed method, incorporating an interface tracking technique, was validated against fundamental physical phenomena, showing agreement with theoretical predictions and computational results. This finding indicates that the proposed method is beneficial for analyzing flow fields containing free surfaces. Through flow analysis around a dolphin kick swimmer using the proposed method, it was clarified that, when considering gravity and free surface deformation, the free surface exhibits an upward displacement in front of the swimmer, a downward displacement directly above the back, and the formation of wave patterns in the wake. A comparison between the results obtained with the proposed method and those from conventional methods demonstrated that the propulsion and drag forces experienced by the swimmer are influenced by variations in the pressure distribution caused by gravity, which results from the free surface shape, and by the arrangement of vortices around the swimmer. Simulations utilizing the proposed method, in which the joint angles and stroke periods of the dolphin kick were varied, revealed that the swimming speed demonstrates a linear relationship with the magnification of angle variation and stroke period variation. The proposed simulation method allows for the analysis required to determine optimal joint angles and stroke periods for improving swimming efficiency.

Disclosure of Interests. The authors have no competing interests to declare that are relevant to the content of this article.

References

1. Counsilman, J.E.: *The Science of Swimming*. Prentice Hall, New Jersey (1968)
2. WORLD AQUATICS Swimming, <https://www.worldaquatics.com/swimming/records>, last accessed 2025/2/25
3. WORLD AQUATICS Rules, <https://www.worldaquatics.com/rules/competition-regulations>, last accessed 2025/2/25
4. Lyttle, A., Blanksby, B.: A look at gliding and underwater kicking in the swim turn. In: 18th International Symposium on Biomechanics in Sports (2000)
5. Nakashima, M.: Simulation analysis of the effect of trunk undulation on swimming performance in underwater dolphin kick of human. *Journal of Biomechanical Science and Engineering* 4(1), 94–1043 (2009)

6. Takagi, H., Shimizu, Y., Kodan, N.: A hydrodynamic study of active drag in swimming. *JSME International Journal, Series B* 42(2), 171–177 (1999)
7. Bixler, B., Riewald, S.: Analysis of a swimmer's hand and arm in steady flow conditions using computational fluid dynamics. *Journal of Biomechanics* 35, 713–717 (2002)
8. Nakashima, M., Satou, K., Miura, Y.: Development of swimming human simulation model considering rigid body dynamics and unsteady fluid force for whole body. *Journal of Fluid Science and Technology* 2(1), 56–67 (2007)
9. Webb, A.P., Taunton, D.J., Hudson, D.A., Forrester, A.I.J., Turnock, S.R.: The effect of swimsuit resistance on freestyle swimming race time. *Procedia Engineering* 72, 709–714 (2014)
10. Cohen, R.C.Z., Cleary, P.W., Mason, B.R.: Simulations of dolphin kick swimming using smoothed particle hydrodynamics. *Human Movement Science* 31(3), 604–619 (2012)
11. Chen, Z., Li, T., Yang, J., Zuo, C.: The effect of the swimmer's trunk oscillation on dolphin kick performance using a computational method with multi-body motion: a case study. *Int. J. Environ. Res. Public Health* 19, 4969 (2022)
12. Ferziger, J.H., Perić, M., Street, R.L.: *Computational Methods for Fluid Dynamics*. Springer (2019)
13. Asao, S., Matsuno, K., Yamakawa, M.: Simulations of a falling sphere with concentration in an infinite long pipe using a new moving mesh system. *Applied Thermal Engineering* 72(1), 29–33 (2014)
14. Yamakawa, M., Matsuno, K.: Unstructured moving-grid finite-volume method for unsteady shocked flows. *Journal of Computational Fluids Engineering* 10(1), 24–30 (2005)
15. Takii, A., Yamakawa, M., Asao, S., Tajiri, K.: Six degrees of freedom flight simulation of tilt-rotor aircraft with nacelle conversion. *Journal of Computational Science* 44, 101164 (2020)
16. Yoon, S.: Lower-Upper Symmetric-Gauss-Seidel method for the Euler and Navier-Stokes equations. *AIAA Journal* 26(9), 1025–1026 (1988)
17. Murayama, M., Nakahashi, K., Matsushima, K.: Unstructured dynamic mesh for large movement and deformation. In: *AIAA Paper 2002-0122* (2002)
18. Yamakawa, M., Mizuno, N., Asao, S., Tanaka, M., Tajiri, K.: Optimization of knee joint maximum angle on dolphin kick. *Physics of Fluids* 32(6) (2020)